Aeolian Research 44 (2020) 100593

Contents lists available at ScienceDirect

Aeolian Research

journal homepage: www.elsevier.com/locate/aeolia

Statistical characterization of sedimentation velocity of natural particles

Lorenzo Raffaele[a,c,*], Luca Bruno[a,c], Douglas J. Sherman[b]

[a] Politecnico di Torino, Department of Architecture and Design, Viale Mattioli 39, I-10125 Torino, Italy
[b] University of Alabama, Department of Geography, AL, 35487 Tuscaloosa, United States
[c] Windblown Sand Modeling and Mitigation Joint Research Group, Italy-France

ARTICLE INFO

Keywords:
Sedimentation velocity
Aerodynamic drag
Natural particles
Statistics
Nonlinear regression
Copula modelling

ABSTRACT

Aeolian sediment transport has major repercussions for global climatic variations, air quality, human health, agricultural areas, air and ground transportation, civil structures and infrastructures. This led to the development of models to understand the involved physical process, and to predict the dynamics of aeolian sediment transport. The sedimentation velocity is one of the key model parameters characterizing sediment behavior. It allows the prediction of the mode of transport, the distribution of particles above the ground, and the sediment transport rate. Despite its importance, there is substantial discrepancy among the sedimentation velocity laws for natural particles, also due to the large dispersion of experimental data. This study proposes the statistical characterization of the experimental measurements of sedimentation velocity available from the literature. 1812 experimental measurements were recovered from 11 studies. Their variability was discussed, providing an aerodynamic reading. Nonlinear regression was carried out on the consolidated dataset in order to assess the average value. Two well-known laws initially conceived for spheres were refitted to natural particles providing high coefficients of determination equal to 0.90 and 0.93. Then, copula-based regression was performed in order to seize the variability of sedimentation velocity. Finally, the results from the two approaches were compared and critically discussed.

1. Introduction

Aeolian sediment transport is an important geomorphological agent of change on many terrestrial and extraterrestrial surfaces. Blowing sand can lead to the development of pans and scour hollows, form a diverse array of landforms that range in scale from ripples to ergs (Pye and Tsoar, 2009), cause abrasion of resistant materials (Paz et al., 2015; Holze and Brucks, 2014), and sand drift can threaten civil structures and infrastructures (Bruno et al., 2018). Blowing dust, often emitted as a consequence of saltating sand, poses a wider set of environmental concerns (Middleton, 2017) because of its potential long-term suspension and capacity for long-distance transport. Blowing dust can transport vital soil nutrients from one location to another, but may also constitute a human health hazard (Griffin, 2007), a traffic hazard for aviation (Baddock et al., 2013) and highway (Li et al., 2018), and impact the radiation balance of the atmosphere (Mass and Portman, 1989; McCormick et al., 1995). For these reasons and many more, there is an abiding interest to develop improved models to understand the fundamentals of aeolian transport, to interpret resulting landforms such as ripples and dunes, to predict the dynamics of sediment transport, to assess the windblown sand risk, and the efficiency of mitigation measures.

Quantifying the characteristics of sediments is a necessary step to model their transport by wind. For a given wind condition in a particular environment, the size, shape, and composition (i.e. density) of a particle will determine if it will be unmoved, or moved by creep, reptation, saltation, suspension, or some combination of those modes of motion. This basic premise is represented in the simplified rubric of sediment diameter and density, as used in most of models for threshold of motion, sand transport rates, and grain trajectories (for example see Nickling and Neuman, 2009; Kok et al., 2012; Ellis and Sherman, 2013; Valence et al., 2015; Baas, 2019). Implicit in these models are the assumptions that sediment size and shape are adequately represented by a single nominal value of particle diameter, and that composition is adequately represented by a single value of density. The sedimentation velocity is, however, a comprehensive, single characteristic of sediments that comprises the influences of, and is function of, particle size, shape, and composition. The sedimentation velocity is commonly defined as the maximum velocity a particle attains if falling unhindered in a quiescent fluid of infinite extent. The terms fall velocity, settling

* Corresponding author at: Politecnico di Torino, Department of Architecture and Design, Viale Mattioli 39, I-10125 Torino, Italy.
E-mail address: lorenzo.raffaele@polito.it (L. Raffaele).
URL: http://www.smart-eid.eu/people/ (L. Raffaele).

https://doi.org/10.1016/j.aeolia.2020.100593
Received 10 October 2019; Received in revised form 3 March 2020; Accepted 9 March 2020
Available online 21 March 2020

velocity, and terminal velocity are often used synonymously with sedimentation velocity, and we will use the latter herein as representing terminal settling velocity.

The estimation of sedimentation velocity is a key modelling issue shared by different scientific communities operating in the fields of fluid mechanics, ecology, powder technology, hydrology, volcanology, geology, and aeolian research, amongst others. In aeolian research, models that include sedimentation velocity are mainly concerned with the prediction of mode of transport, distribution of particles above a surface, and sediment transport rates. Critical values of the ratio of sedimentation velocity to shear velocity, for example, have been described as representing transition thresholds from one mode of transport to another, such as from saltation to suspension on Earth and Mars (e.g. Sundborg, 1955; White et al., 1997; Jerolmack et al., 2006; Kok and Renno, 2009). In a similar vein, sedimentation velocity has been used to describe vertical concentration profiles, dating back to the original work of Rouse (1938b) and applied in air by Ishihara and Iwagaki (1952), Anderson and Hallet (1986), Udo and Mano (2011), Farrell and Sherman (2013), among others. Some approaches to sediment transport modeling also rely on a sedimentation velocity term to different extents. For instance, the transport rate models of Owen (1964) and Pischiutta (2012) replace the particle diameter with sedimentation velocity, because the latter integrates more information about the dynamic behavior of a particle than does its purely geometric metric. Several saltation models include the sedimentation velocity, e.g. Ji et al. (2004), Kok and Renno (2009), Wang et al. (2014), Preziosi et al. (2015). Further, there is a large literature discussing the influences of sedimentation velocity on aeolian dust transport and deposition (e.g. Gillies, 2013; McTainsh et al., 2013; Marticorena and Formenti, 2013; Fernandes et al., 2019) and microfauna (e.g. Rivas et al., 2018).

The fundamental role of the sedimentation velocity in the models above, and the difficulty in attributing experimental estimates, motivate the development of robust laws to relate sedimentation velocity to particle characteristics. If all particles were spherical, the sole diameter would be relevant, and there would be little controversy concerning the correct model, given the negligible variability in measurements (Brown and Lawler, 2003). Conversely, there is substantial ambiguity between the different laws that consider natural particles. The wording natural particle is used herein as a synonym of non-spherical, irregularly-shaped (i.e. with non-symmetric rough surface) particle (Loth, 2008). Overall, two kinds of modelling approach to assess the sedimentation velocity (or its aerodynamic drag counterpart) exist, that is *size-dependent* laws (e.g. Farrell and Sherman, 2015 and references therein), and *size and shape-dependent* laws (e.g. Bagheri and Bonadonna, 2016 and references therein). The latter define the particle shape by one or more descriptors referred to an equivalent ellipsoid, and need time-consuming laboratory procedures merging particle analysis and image analysis for each particle (Wang et al., 2018). Regardless of the modelling approach, all these laws remain purely deterministic, and do not allow to completely reflect the large variability in measurements (Farrell and Sherman, 2015). Such a variability stems from different causes that can be categorized according to a general and recent classification of the uncertainties (Zio and Pedroni, 2013). Measurement uncertainties are due to measurements errors and to heterogeneous experimental procedures. For instance, Farrell and Sherman (2015) and Brown and Lawler (2003) systematically and critically discuss the effects of fall column height and diameter on the available measurements for particle sizes that might vary over several orders of magnitude, respectively. Aleatory uncertainty mainly includes particle irregularities, such as shape and surface roughness. Indeed, according to Loth (2008), "[…] *the shape characterization of the particles is often not documented (e.g. a study may mention simply that sand particle of an effective diameter was used) and is generally difficult to measure*", and "[…] *irregularity generally leads to random protuberances orientations so that the statistical variation of the drag is often large*". This motivates our re-examination of existing data to refit existing well-established laws, and to develop a novel statistical characterization of the sedimentation velocity based on copula regression.

The paper is organized in five further sections. Section 2 briefly reviews the equilibrium of freely falling particles, collects a number of experimental measurements from the literature and critically analyzes them. In Section 3, nonlinear regression is applied to the dataset and the average sedimentation velocity for aeolian particles is recovered. Copula-based regression is described and applied in Section 4 and the results are discussed and compared in Section 5. Finally, conclusions and perspectives are outlined in Section 6.

2. Background on falling particles

A single particle falling in any quiescent Newtonian fluid accelerates until it reaches a constant velocity when equilibrium conditions are met. Experimental procedures rely upon the direct measurement of the particle diameter and the equilibrium sedimentation velocity.

2.1. Physical model

The single falling particle is subjected to three fundamental forces: drag F_d, gravity F_g, and buoyancy F_b (see Fig. 1). They are commonly expressed as

$$F_d = \frac{1}{2}\rho_f \omega^2 C_d \frac{\pi d^2}{4} \tag{1}$$

$$F_g = \rho_p g \frac{\pi d^3}{6} \tag{2}$$

$$F_b = \rho_f g \frac{\pi d^3}{6}, \tag{3}$$

where ρ_p is the particle density, ρ_f is the fluid density, g is the acceleration of gravity, C_d is a drag coefficient, ω is the fall velocity, and d the equivalent particle diameter (i.e., the diameter of a sphere with the same volume as the natural particle). At equilibrium the fall velocity ω in Eq. (1) is equal to the sedimentation velocity ω_s, and the following well known equality holds:

$$F_d = F_g - F_b. \tag{4}$$

By substituting Eqs. (1)–(3) into Eq. (4), the drag coefficient can be obtained as:

$$C_d = \frac{4(\rho_p - \rho_f) g d}{3\rho_f \omega_s^2}. \tag{5}$$

By substituting the particle Reynolds number Re into Eq. (5), one transforms measurements into dimensionless quantities:

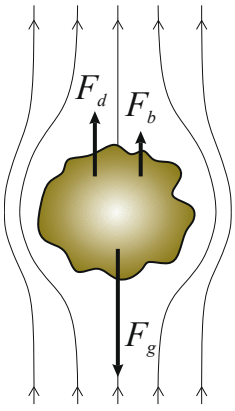

Fig. 1. Forces acting on a falling particle.

$$\begin{cases} \mathrm{Re}=\frac{\omega_s d}{\nu_f} \\ C_d = \frac{4}{3}\frac{\rho_f(\rho_p-\rho_f)}{\mathrm{Re}^2\mu_f^2}gd^3, \end{cases} \quad (6)$$

where ν_f and μ_f are the kinematic and the dynamic viscosity of the fluid, respectively. The dimensionless pair of Re and C_d is the form traditionally used to compare the measured values for d and ω_s (Rouse, 1938a). Alternatively, other studies adopt different but perfectly equivalent dimensionless forms (see e.g. Dietrich, 1982; Le Roux, 2014 and cited references). Finally, it is worth remarking that given the dimensionless pair of Re and C_d, the corresponding dimensional forms d and ω_s can be recovered by inverting the transformation in Eq. (6) as:

$$\begin{cases} d = \left[\frac{3}{4}\frac{C_d\mathrm{Re}^2\mu_f^2}{\rho_f(\rho_p-\rho_f)g}\right]^{1/3} \\ \omega_s = \frac{\mathrm{Re}\,\nu_f}{d}. \end{cases} \quad (7)$$

2.2. Data collection and aerodynamic regimes

The experimental apparatus to measure the sedimentation velocity and the drag coefficient of freely falling natural particles has improved over the years, from the first pioneering studies of Bagnold (1935), to the most recent ones of Wang et al. (2018). The most common setup includes a fall column (i.e. settling tube) filled with fluid (gas or liquid) at controlled temperature and pressure. The particle sample is dropped at the top, and the falling time is measured by means of a weighting apparatus at the bottom (Shao, 2008). In recent times, the particle sedimentation is recorded by high-resolution cameras allowing the direct particle velocity measurement by means of particle tracking techniques (e.g. Wang et al., 2018).

In this study, experimental data are mapped on the dimensionless plane Re-C_d through Eq. (6) in order to homogenize measurements obtained in different Newtonian fluids (air, water, glycerine, oil) and for different particle densities so to expand the cardinality of the dataset and make it suitable for application by different scientific communities. Moreover, the Re-C_d plane highlights the behavior of the falling particles by referring to well-established aerodynamic regimes (Stokes, Newton and intermediate regimes, as in Achenbach, 1974; Johnson and Patel, 1999). This provides a physical basis for the statistical treatment of the data. The resulting dataset for natural particles is plotted in Fig. 2(a). The colours correspond to the nature of the fluid, while the symbols correspond to the experimental campaign. The high quality Re-C_d dataset for smooth spheres collected by Brown and Lawler (2003) and their aerodynamic regimes are included for reference only in Fig. 2(a) and (b), respectively.

The present study addresses the careful collection of sedimentation velocity measurements from the literature, and it is not intended to provide new experimental measurements. The dataset includes two main sub-ensembles: sand grains falling in air, and natural particles falling in other fluids. Recently, Farrell and Sherman (2015) collected all available ω_s measurements of *sand grains falling in air* from the past literature. They identified five studies, resulting in a collection of 352 distinct measurements from Bagnold (1935), Wilson and Huang (1979), Cui et al. (1983), Malcolm and Raupach (1991), Chen and Fryrear (2001). The dataset is then complemented by Re-C_d measurements of *natural particles falling in fluids of different densities and viscosity*. Overall, 911 measurements of particles of different sizes and densities falling through water, solutions of glycerine and water, and oil are obtained from the sources reported in the popular study of Dietrich (1982), i.e. Corey (1949), Wilde (1952), Schulz et al. (1954), Briggs et al. (1962), Alger (1964), Romanovskiy (1966), Stringham et al. (1969), Komar and Reimers (1978). In addition, the high-cardinality Re-C_d measurements of volcanic deposits (304) and calcareous sand particles (521) falling through solutions of glycerine and water are obtained from the recent studies of Dioguardi et al. (2017) and Wang et al. (2018), respectively. From Fig. 2, the C_d of natural particles is generally more scattered than that for smooth spheres, consistent with findings in the literature (e.g. Loth, 2008; Bagheri and Bonadonna, 2016). Spheres are basically deployed along a curve, while the scatter for natural particles increases as Re increases. Moreover, C_d of the vast majority of natural particles is larger than that for spheres for the same Re. The test in fluids of different densities and viscosities provides C_d measurements covering the range $10^{-2} < \mathrm{Re} < 10^5$, and the corresponding aerodynamic regimes. These are briefly reviewed in the following and related to the well-known aerodynamic behavior of smooth spheres (Fig. 2b):

- Within *Stokes' regime* (Re < 20–25), the inertial terms are globally negligible with respect to the viscous ones. The laminar boundary layer is fully attached to the sphere (Fig. 2b, panel 1). The wake is fully symmetric and steady without any recirculation region. As a result, C_d is expected to be insensitive to the particle surface roughness (Loth, 2008). However, at a given Re, the C_d of natural particles is higher than that for spheres. This is caused by the increased surface with respect to a sphere with the same equivalent diameter (Loth, 2008), and the tendency of a particle to orient with the largest projection area normal to the sedimentation direction (Cox, 1965).
- Within the *intermediate regimes* (20–25 < Re < 1000–2000), the laminar boundary layer is detached from the sphere. However, very different wake patterns occur, and the transition from one to another is not sharp even for nominal spheres, as testified by the overlapping between successive regimes (Fig. 2b, panels 2–4). Steady, axisymmetric, topologically similar wakes grow behind spheres up to Re ≈ 130–300 in the form of a ring vortex, extending from $0.5d$ to $1.5d$ as Re increases from 50 to 200 (Johnson and Patel, 1999). Then, the steady wake becomes non-axisymmetric up to Re ≈ 270–420. Symmetry still exists in the $x-z$ plane, even if the streamlines have out of plane components. The $x-y$ plane highlights that the vortex is no longer a closed separation bubble and streamlines follow a 3d spiral path. Finally, the wake becomes unsteady at about 270 < Re < 2000. Vortex shedding in the from of the so-called hairpin vortices occurs (Achenbach, 1974). For Re approaching 2000, laminar-to-turbulence transition progressively occurs in the wake, even if coherent, large-scale wake structures still hold (Tomboulides and Orszag, 2000). At a given Re within intermediate regimes, the C_d of natural particles is expected to be higher than the one occurring for smooth spheres (Loth, 2008), even if a precise phenomenological reading is not straightforward because of the flow complexity.
- Within *Newton's regime* (1000–2000 < Re < $3.7e+5$), the flow viscous terms become globally negligible with respect to the inertial ones. The separation of the laminar boundary layer occurs, laminar-to-turbulence transition takes place downstream the separation point, and irregular vortex shedding develops in the wake (Fig. 2b, panel 5). Within this range, the separation point of spheres does not move, and C_d is almost constant. Both the overall shape and the surface irregularities of natural particles affect the position of the separation point and C_d. According to Loth (2008), effects induced by non-spherical shapes may be attributed to the increased sensitivity of boundary layer separation to increased shape convolutions. Effects induced by local irregularities are ascribed to local high curvatures of the surface that induce the early boundary layer separation, the wider wake and the higher C_d. Furthermore, as Re increases, the sedimentation pattern is chaotic and tumbling (Bagheri and Bonadonna, 2016) resulting in a greater dispersion of measurements.

We critiqued the fall velocity datasets to remove potentially unreliable Re-C_d measurements, and discarded those for the following reasons (see gray-colored symbols in Fig. 2a). In particular:

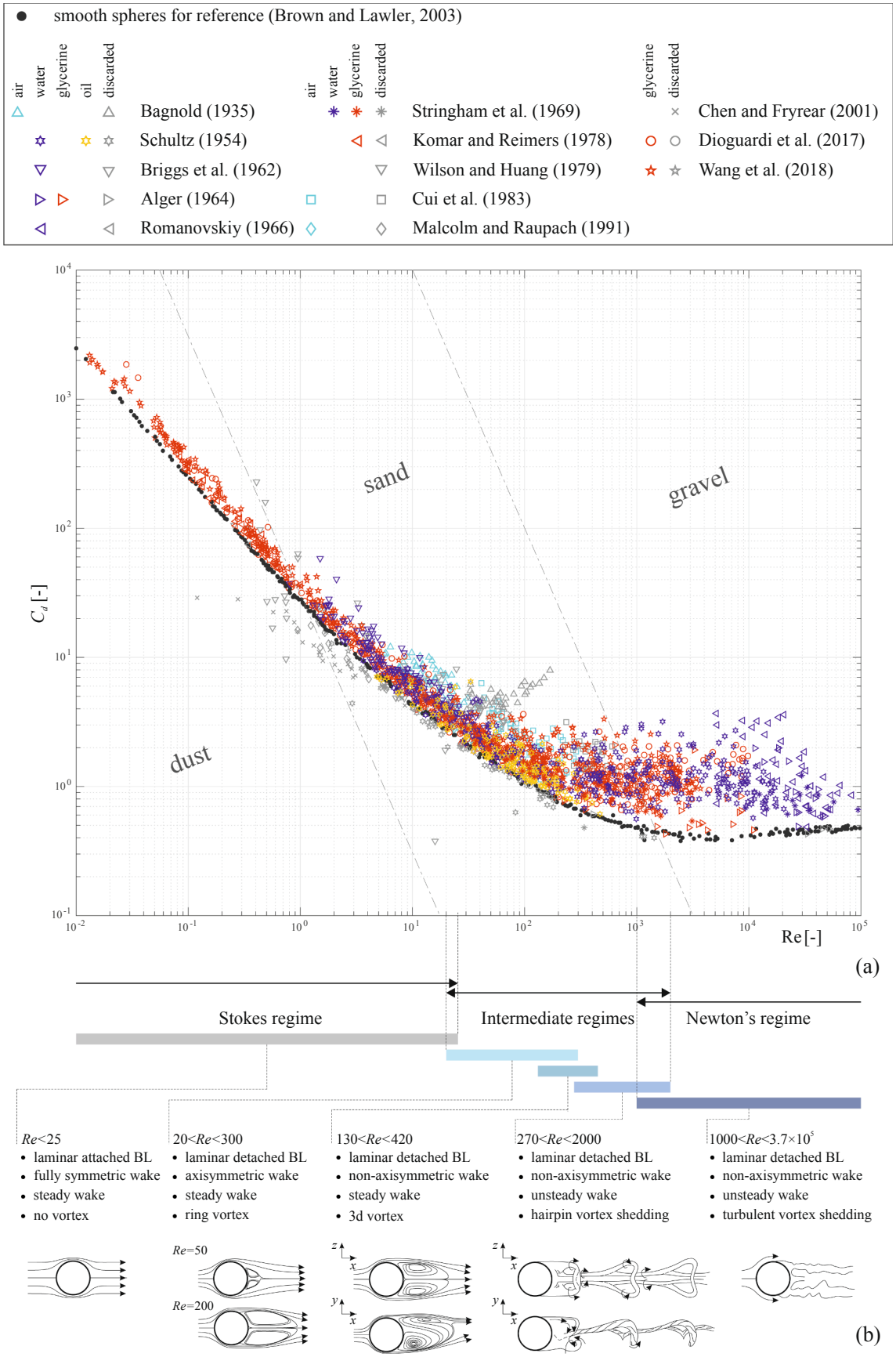

Fig. 2. (a) Measurements of drag coefficient versus particle Reynolds Number for natural particles and smooth spheres. (b) Smooth spheres aerodynamic regimes and corresponding structure of the flow after Achenbach (1974) and Johnson and Patel (1999).

- some experiments did not adopt a fall height equal to or greater than the critical falling height, i.e. the required height to reach the sedimentation (terminal) velocity. This leads to underestimating the sedimentation velocity and overestimating the drag coefficient. Such conditions were previously identified by Farrell and Sherman (2015) in Bagnold (1935), Wilson and Huang (1979), Cui et al. (1983), Malcolm and Raupach (1991), Chen and Fryrear (2001).
- some experiments tested spherical particles. Such measurements are not included because they are outside the scope of this study except as described above for comparative purposes. Spheres have been tested in Alger (1964), Stringham et al. (1969), Malcolm and Raupach (1991), Chen and Fryrear (2001).
- the results obtained by Chen and Fryrear (2001) are not included herein for two main reasons. First, some studies questioned their validity, see e.g. Roux (2002), Chen and Fryrear (2002), or Le Roux (2005). Secondly, those measurements are much different from those of other experiments, with no apparent rationale (see Fig. 2a).
- a few pairs of Re and C_d measurements fall just below those found for spheres within the Stokes and intermediate regimes. Such outcomes could be caused by measurement errors or partially uncontrolled experimental procedures. In the following, all the Re-C_d measurements less than those for equivalent spheres are discarded in order to define a physically sound dataset, in agreement with the well-established aerodynamic concepts detailed above.

The datasets used for our final analysis are summarized by source in Table 1, including the particle diameters and densities, and subset cardinality numbers #. The total number of the Re and C_d pairs used is 1812.

For reference to aeolian applications, the Re-C_d plane in Fig. 2 is mapped into three regions, corresponding to dust $0.01 < d < 0.063$ mm, sand $0.063 < d < 2$ mm, and gravel $d > 2$ mm size particles according to ISO14688-1 (2017) categorization. The mapping follows from Eq. (6) and by referring to quartz particles falling in air ($\rho_p = 2650$ kg/m^3, $\rho_f = 1.23$ kg/m^3, $\mu_f = 1.84e-5$ kg/ms, $\nu_f = 1.5e-5$ m^2/s). From such a mapping, it clearly emerges that: (i) blown dust particles fall within the Stokes regime; (ii) windblown sand particles are subjected to both Stokes and intermediate regimes; and (iii) Newton's regime includes gravel particles in the granule size range and greater, such as those observed in megaripples (e.g. Yizhaq and Katra, 2015).

3. Nonlinear regression

In the literature, a number of C_d laws for spheres exist (e.g. Clift and Gauvin, 1971; Haider and Levenspiel, 1989; Brown and Lawler, 2003; Clift et al., 2005). Among these, the law of Clift and Gauvin (1971) is the most widely used, and it is considered by Bagheri and Bonadonna (2016) to be one of the most accurate in the Re intervals of interest, and it reads:

$$C_d = \frac{24}{\mathrm{Re}}(k_{S1} + k_{S2}\mathrm{Re}^{k_{S3}}) + \frac{k_{N1}}{1 + \frac{k_{N2}}{\mathrm{Re}^{k_{N3}}}} \quad \text{for} \quad \mathrm{Re} < 3.7{\cdot}10^5 \tag{8}$$

where
$k_{S1} = 1$, $k_{S2} = 0.15$, $k_{S3} = 0.687$, $k_{N1} = 0.42$, $k_{N2} = 42500$, $k_{N3} = 1.16$. Similarly, a number of C_d laws for natural particles exist (e.g. Haider and Levenspiel, 1989; Ganser, 1993; Tran-Cong et al., 2004; Bagheri and Bonadonna, 2016; Dioguardi et al., 2017; Wang et al., 2018). Most of these are defined on the basis of the existing C_d laws for spheres by introducing particles shape correction factors. Recently, Bagheri and Bonadonna (2016) proposed a new, relatively simple law for natural particles by defining two shape-dependent parameters called Stokes' drag correction k_S and Newton's drag correction k_N:

$$C_d = \left\{ \frac{24\,k_S}{\mathrm{Re}\,k_N}\left[1 + 0.125\left(\mathrm{Re}\frac{k_N}{k_S}\right)^{2/3}\right] + \frac{0.46}{1 + \frac{5330}{\mathrm{Re}\,k_N/k_S}} \right\} k_N \tag{9}$$

In this study, Eqs. (8) and (9) are fitted to the Re-C_d dataset through a nonlinear regression by considering k_S and k_N as free parameters. The regression analysis allows the estimation of the average value of the dependent variable C_d for fixed values of the independent variable Re, by providing an estimate of each free parameter. Fig. 3 shows the Re-C_d data with original drag laws for spheres, i.e., the laws by Stokes (1851) with $C_d = 24/\mathrm{Re}$, Newton (1687) with $C_d \approx 0.46$, and Clift and Gauvin (1971), and fitted laws for natural particles. The estimated parameters for Eq. (8) correspond to $k_{S1} = 0.2951$, $k_{S2} = 0.6395$, $k_{S3} = 1.24$, $k_{N1} = 0.8327$, $k_{N2} = 9849$, $k_{N3} = 1.4104$. For Eq. (9), they are and $k_S = 1.2807$, $k_N = 2.6893$. The two curves are perfectly overlapped up to Re = 300. After that, they show different trends. In particular, Eq. (8) better follows the data for very high Re because of the large number of free parameters. Conversely, Eq. (9) conserves the typical trend of $C_d(\mathrm{Re})$ for spheres resulting in higher C_d for very high Re.

In Fig. 4, the Re-C_d dataset and the laws plotted in Fig. 3 are made dimensional through Eq. (7) in the plane d-ω_s, by standardizing for quartz particles falling in air. Fig. 4 is complemented with some of the best performing $\omega_s(d)$ laws for spheres and natural particles (see Le Roux, 2014; Farrell and Sherman, 2015 and cited references), i.e. the laws of Cui et al. (1983) and Le Roux (2014) for spheres, the ones proposed by Cui et al. (1983) and Farrell and Sherman (2015) for sand only, and the ones of Ferguson and Church (2004) and Le Roux (2014) for natural particles of any diameter. It is worth highlighting that the law of Le Roux (2014) coincides almost exactly with the sedimentation velocity derived on the basis of the $C_d(\mathrm{Re})$ law of Clift and Gauvin (1971). The law of Cui et al. (1983) behaves similarly, apart for large diameters. As far as the sedimentation velocity of natural particles is concerned, Eqs. (8) and (9) best fit the data for all diameters, while the other laws have analogous performances only locally, e.g. Cui et al. (1983) for medium sand, and Ferguson and Church (2004) for gravel. The law by Le Roux (2014) deviates from data for gravels at $d \approx 4{\cdot}10^{-3}$ m: we believe that such trend is mainly due to the 5th-order polynomial law, and to the narrow range of particle diameters considered for fitting. The linear law proposed by Farrell and Sherman (2015) has the simplest form, but provides local over and underestimation.

The goodness of fit of the laws for natural particles plotted in Fig. 4 is given in Table 2 in terms of coefficient of determination R^2, by referring to sand-sized particles only (left column) and the whole domain (right column). As far as sand-sized particles are concerned, all the laws perform relatively well. In particular, the predictions of both the fitted Eqs. (8) and (9) as well as the law of Ferguson and Church (2004) score the highest $R^2 \approx 0.92$. Conversely, when referring to all particles size, the fitted Eq. (8) and Ferguson and Church (2004) perform better than the rest ($R^2 \approx 0.93$).

Table 1
Details of the retained datasets .

Source	Particle nature	d [mm]	ρ_p [kg/m^3]	#
Bagnold (1935)	desert sand	[0.139, 0.334]	2650	62
Schulz et al. (1954)	fluvial sediment	[0.2, 7.07]	2579–7500	492
Briggs et al. (1962)	sedimentary rocks	[0.07, 0.46]	3190–5070	125
Alger (1964)	sedimentary gravels	[24.4, 33.1]	2570–2980	59
Romanovskiy (1966)	fluvialsediment	[9.8, 74]	2220–2980	52
Stringham et al. (1969)	steel and aluminium spheroids	[12.3, 31.2]	2810,10150	79
Komar and Reimers (1978)	basalt pebbles	[7.23, 19.86]	3011	51
Cui et al. (1983)	beach sand	[0.36, 1.072]	2650	58
Malcolm and Raupach (1991)	sand	[0.138, 0.459]	2610	14
Dioguardi et al. (2017)	volcanic deposits	[2.18, 22.97]	813–1235	303
Wang et al. (2018)	calcareous sand	[2.9, 9.7]	1614–2833	517

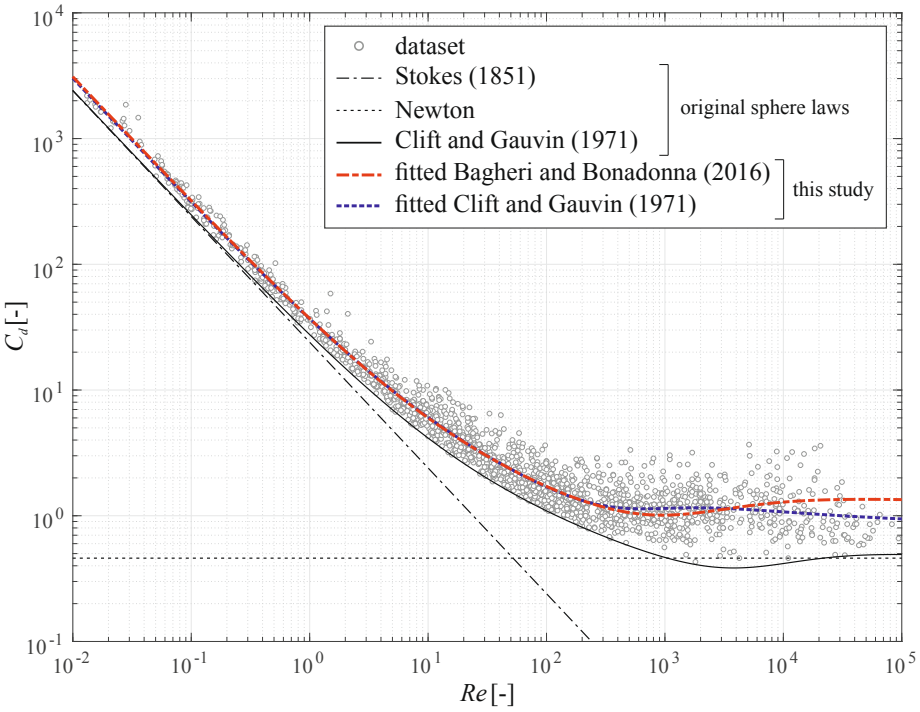

Fig. 3. Nonlinear regression of Eqs. (8) and (9) on Re-C_d plane.

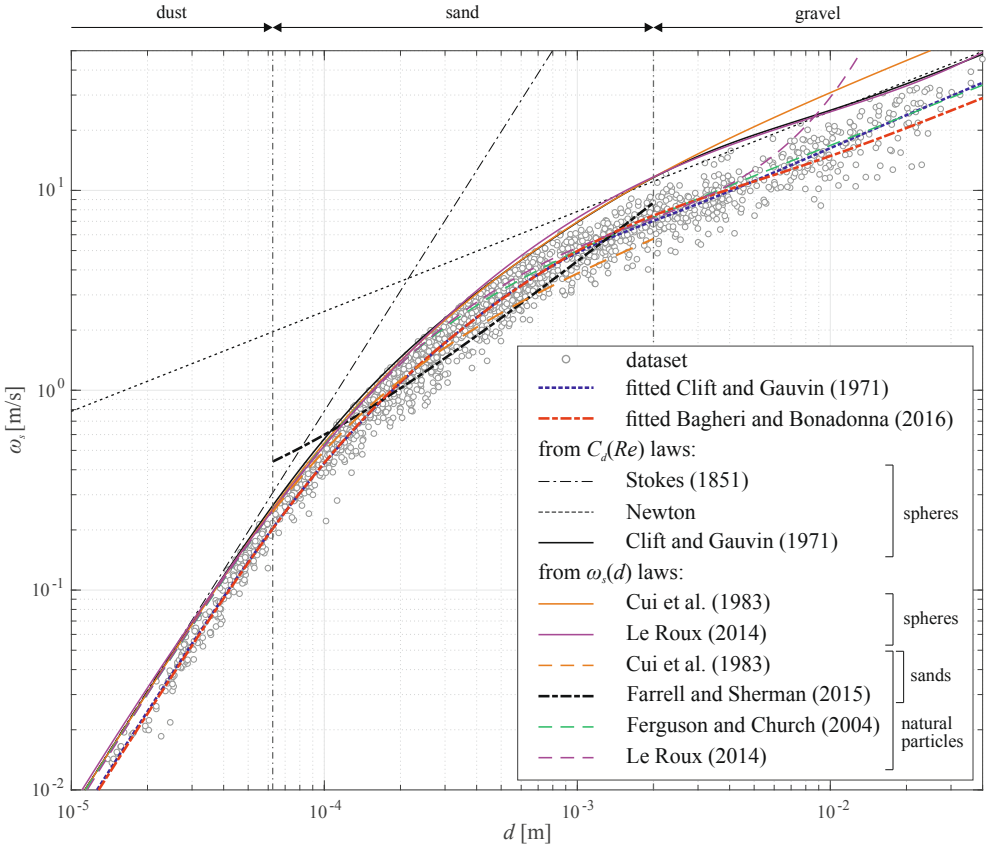

Fig. 4. Comparison between fitted laws and literature laws of the sedimentation velocity of quartz particles falling in air.

Table 2
Coefficient of determination R^2 on d-ω_s plane.

	sand ($6.3 \cdot 10^{-5} < d < 2 \cdot 10^{-3}$ m)	all particles ($10^{-5} < d < 4 \cdot 10^{-2}$ m)
fitted Clift and Gauvin (1971)	0.9228	0.9310
fitted Bagheri and Bonadonna (2016)	0.9284	0.8927
Cui et al. (1983)	0.8247	–
Ferguson and Church (2004)	0.9198	0.9288
Le Roux (2014)	0.8944	0.0577
Farrell and Sherman (2015)	0.8807	–

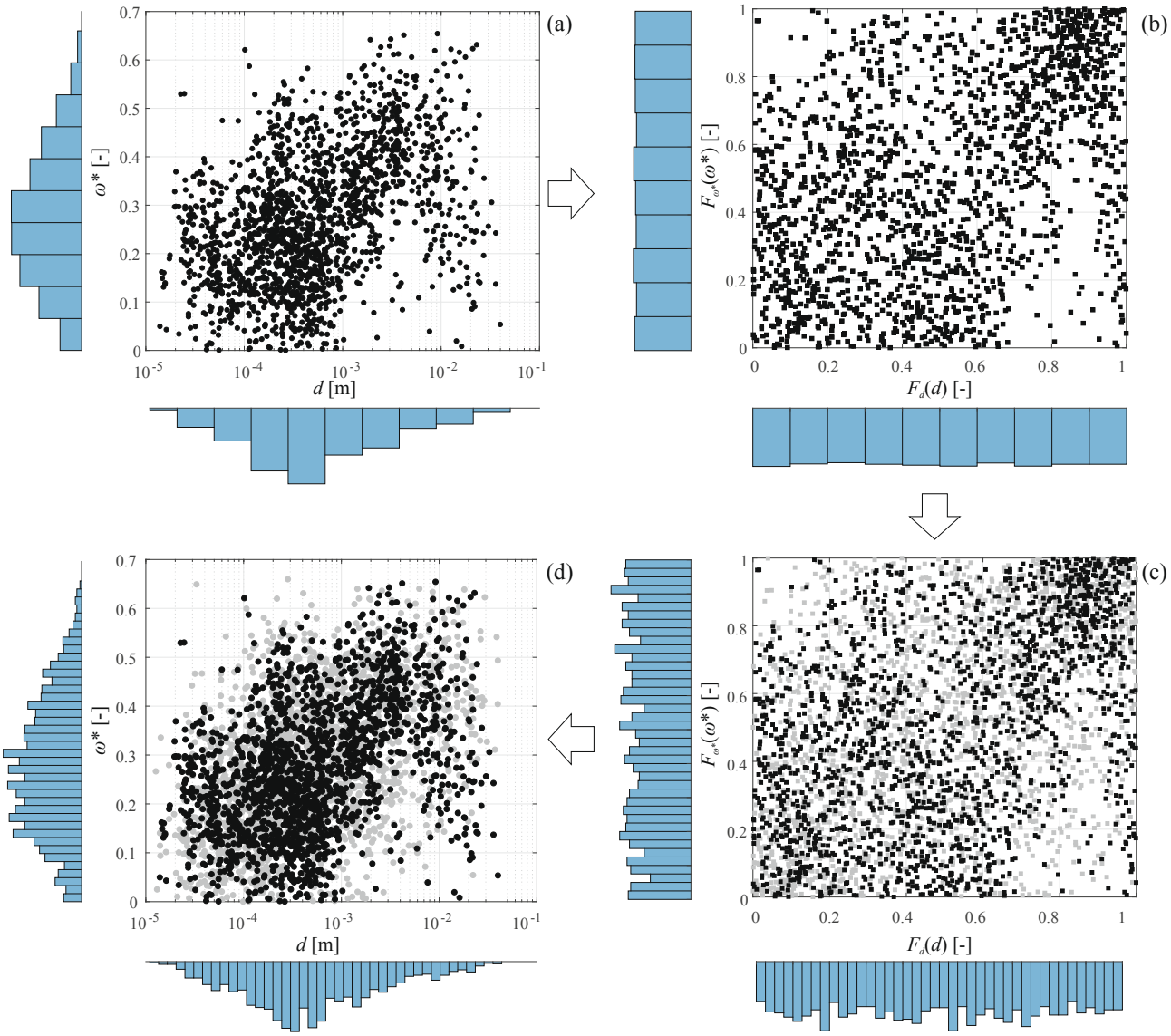

Fig. 5. Copula fitting procedure: (a) experimental dataset; (b) scatter plot of the pairs $(F_d(d), F_{\omega^*}(\omega^*))$; (c) random sample from Frank copula; (d) resizing to the original scale of the experimental dataset. Experimental dataset is plotted in black, while copula generated samples are plotted in gray. The same pairs are drawn as dots on the $d - \omega^*$ plane, and as squares on the $F_d(d) - F_{\omega^*}(\omega^*)$ plane.

4. Copula-based regression

In the light of the uncertainties discussed in Section 1, and of the highly scattered measurements of ω_s for natural particles observed in Section 2.2, a copula-based regression is performed. Such an approach accommodates the variability of ω_s for given values of d, by means of statistical moments other than the mean, and with percentiles. For the sake of brevity, the copula-based regression is briefly outlined as a complete description of the copula modelling and quantile regression is out of the scope of the present paper. Interested readers can refer to e.g. Genest and Favre (2007) and Raffaele et al. (2016), where the copula modelling is used to investigate the dependence between analogous random environmental variables.

Within the copula modelling, both d and ω_s are considered to be random variables. The copula modelling is carried out on the bivariate joint density function described by the marginal densities $f(d)$ and $f(\omega^*)$, being $\omega^* = (\omega_{s,sphere} - \omega_s)/\omega_{s,sphere}$ where $\omega_{s,sphere}$ is the sedimentation velocity of a sphere with same equivalent diameter d. The

Table 3
Tested copulas sorted by ranking and associated Root Mean Square Error.

Rank	Copula name	RMSE
1	Frank, Nelsen	0.6088
2	Plackett	0.6339
3	Gaussian	0.6755
4	t	0.6829
5	Roch-Alegre	0.6897
6	Tawn	0.7010
7	BB1	0.7017
8	BB5, Galambos, Gumbel	0.7019
9	Burr	0.7450
10	Fischer-Hinzmann	0.7667
11	Marshal-Olkin	0.7735
12	FGM	0.7739
13	Fischer-Kock	0.7740
14	Cuadras-Auge	0.7772
15	Joe	0.7954
16	Linear-Spearman, Shih-Louis	0.8400
17	AMH	0.8421
18	Clayton	0.9374
19	Raftery	1.0475
20	Cubic	1.9749
21	Independence	1.9985

scatter plot of the (d, ω^*) pairs, as well as their empirical marginal densities are plotted in Fig. 5(a). The joint cumulative distribution of the $(F_d(d), F_{\omega^*}(\omega^*))$ pairs, as well as their uniform marginal distributions, are plotted in Fig. 5(b). The joint cumulative distribution can be written as

$$F(d, \omega^*) = C\{F_d(d), F_{\omega^*}(\omega^*)\}, \quad d \in \mathbb{R}^+, \ \omega^* \in [0, 1] \tag{10}$$

where F_d and F_{ω^*} are the cumulative marginal distributions of d and ω^*, respectively, and C: $[0, 1]^2 \rightarrow [0, 1]$ is the copula of the pair (d, ω^*). It is worth stressing that the support of ω^* is bounded between 0 and 1 since $\omega_s \leqslant \omega_{s,sphere}$.

The copula C provides the dependence structure between the random variables d and ω^*, by establishing their correlation and by discarding the effect of their marginal distribution. Several copulas have been proposed in the literature. Interested readers can refer to Nelsen (2007), for a complete review. Generally, the choice of the copula can be performed by visually comparing the $F_d(d) - F_{\omega^*}(\omega^*)$ scatter plot of the observed dataset to an artificial dataset generated from the fitted copula (Genest and Nešlehová, 2014), as done by Raffaele et al. (2016). In this study, a goodness of fit quantitative assessment is carried out. It is based on the rigorous numerical methodology recently proposed by Sadegh et al. (2017) and implemented in the MvCAT toolbox. Table 3 reports the 25 tested copulas sorted by the overall ranking on the basis of the Root Mean Square Error (RMSE).

The Frank and Nelsen copulas produce the lowest RMSE. In this study, the Frank copula is chosen because of its performance in this test and because its use is widespread. The Frank copula is defined as follows:

$$C(u, v) = -\frac{1}{\alpha}\ln\left[1 + \frac{(\exp(-\alpha u) - 1)(\exp(-\alpha v) - 1)}{\exp(-\alpha) - 1}\right], \quad u, v \in [0, 1], \alpha \in \mathbb{R}\backslash 0 \tag{11}$$

where $\alpha = 2.72$ is the best fitting parameter. In Fig. 5(c), a 3000 point sample is generated with the Frank copula. This replicates the quasi symmetric tail dependence in the lower-left and upper-right corners, i.e. close to (0, 0) and (1, 1). However, a slight discrepancy between the Frank copula-generated sample and the original dataset remains in the lower-right corner, i.e. close to (1, 0) in Fig. 5(c). This is because the scatter plot of the original dataset is slightly asymmetric with respect to the bisector, while the Frank copula is symmetric. $C(u, v)$ is transformed back into the original units by inverting the cumulative marginal distributions as $(d, \omega^*) = (F_d^{-1}(d), F_{\omega^*}^{-1}(\omega^*))$. Fig. 5(d) shows the original experimental dataset with the copula generated sample in the original d-ω^* plane. Both the (d, ω^*) copula generated pairs and the corresponding empirical marginal distributions show a good overall match with those related to the original dataset.

Finally, (d, ω_s) pairs and related statistics are derived from the obtained copula generated sample (d, ω^*). The size of the copula-generated sample is increased up to 10^7 in order to post-process the joint probability density function $f(d, \omega_s)$. Fig. 6(a) plots the resulting conditional densities $f(\omega_s|d)$ of the sedimentation velocity for given values of diameter together with the original dataset. Fig. 6(b) and (c) plot the corresponding trend of the coefficient of variation (*c. o. v.*) and skewness (*sk*) of $f(\omega_s|d)$, respectively.

It is worth noting that the *c. o. v.* and *sk* show the same general trend: they increase with increasing d. Overall, ω_s increases its variability up to non-negligible values (*c. o. v* ≈ 0.2), by preserving a

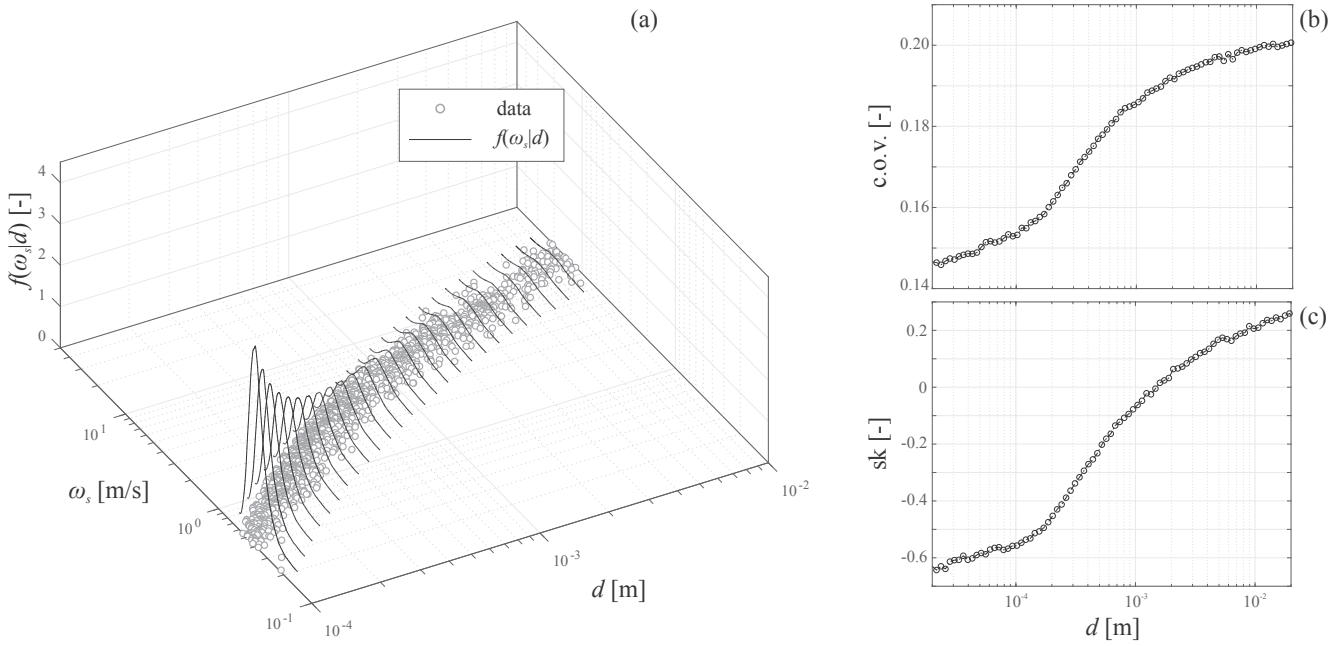

Fig. 6. Copula-based regression of ω_s: (a) conditional densities of ω_s for given values of d; (b) coefficient of variation; (c) and skewness.

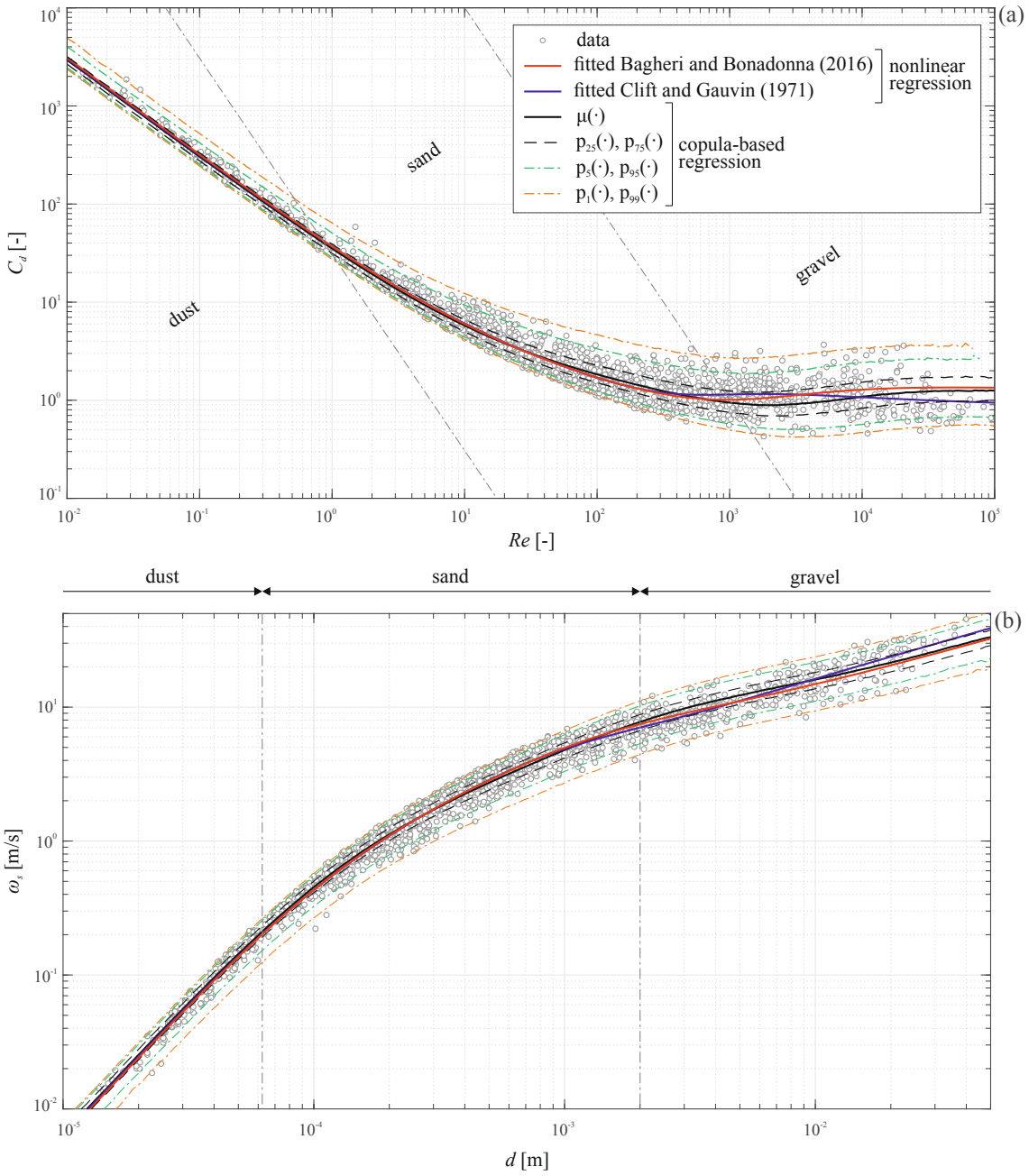

Fig. 7. Comparison between the results obtained from nonlinear regression and copula-based regression on the Re-C_d (a) and $d - \omega_s$ (b) planes.

quasi-symmetric distribution ($sk \in [-0.55, 0.2]$) in the range $10^{-4} < d < 10^{-2}$ m.

5. Comparative analysis

The results obtained through the nonlinear regression (Section 3) and copula-based regression (Section 4) are compared. Fig. 7(a) plots on the Re-C_d plane the fitted laws resulting from the nonlinear regression, the mean value μ and i-th percentiles of the drag coefficient $p_i(C_d)$ for $i = \{1, 5, 25, 75, 95, 99\}$ from the copula-based regression, and the original dataset. Fig. 7(b) plots the same curves and dataset on the d-ω_s plane by referring to quartz particles in air. Indeed, it is straightforward to pass between the two planes thanks to Eqs. (6) and (7).

From the comparison of results, it emerges that $\mu(C_d)$ and $\mu(\omega_s)$ follow almost exactly the fitted laws of Clift and Gauvin (1971) and Bagheri and Bonadonna (2016) up to Re < 500 and $d < 10^{-3}$ m, respectively. After that, they slightly depart from each other, with the relationship found by Bagheri and Bonadonna (2016) tending again to the mean value for high Re and d. The copula-based regression enriches the description of C_d and ω_s, by taking into account and quantifying the measured variability of C_d and ω_s for given values of Re and d, respectively. Extreme percentiles effectively bracket the majority of the data by following their overall trend. It is worth noting that the local accuracy of both non-linear and copula regressions are presumably diminished by the paucity of data for extreme values of Re and d.

6. Conclusions

Accurately characterizing the sedimentation velocity of natural particles is important for many aeolian modeling applications. In practice, the sedimentation velocity of natural particles may be assessed by means of direct experimental measurement, or through the

definition of analytical laws as a function of the particle size. There are challenges with both approaches. On the one hand, experimental measurements requires special expertise and dedicated instrumentation not always available, especially in the context of practical engineering applications. On the other hand, there is substantial discrepancy in the predictions made by the different sedimentation velocity laws. These challenges underpin the motivation to attempt a copula-based approach to include a statistical representation of the natural variability in the data describing drag coefficients and sedimentation velocities.

The proposed statistical characterization is based on the collection of a wide dataset of experimental measurements from the literature. As a result, the data comprise different kinds of natural particles, from aeolian sand grains to volcanic particles. The distributions of the data were first compared to a well-controlled data set and model that predicts the well-known aerodynamic behavior of smooth spheres. Two well-established drag laws were fit to the data with common nonlinear regression, and their goodness of fit was assessed by reference to other well-known laws for natural particles. Despite their overall goodness of fit, they merely describe the average trend and do not provide any information about the variability of the sedimentation velocity. Hence, a copula-based regression was performed to provide the trend of high order statistics and extreme percentiles. The proper definition of drag coefficient and sedimentation velocity as values associated with a given probability density can account for the random variations of shape, orientation, and roughness between grains in the absence of quantitative descriptions. This paves the way toward the probabilistic modelling of aeolian sediment transport.

From this work we can draw three conclusions:

1. Based upon analysis of the results of the non-linear regression assessments of d and ω_s for sand-sized particles, the fitted models of Clift and Gauvin (1971) and Bagheri and Bonadonna (2016) and the general model of Ferguson and Church (2004) provide excellent estimates of sedimentation velocity based on grain size alone. Each of those laws has a coefficient of determination of 0.92 or better.
2. For the broader range of particle sizes from 10^{-5} to $4{\cdot}10^{-2}$ m, the fitted model of Clift and Gauvin (1971) and the Ferguson and Church (2004) model produce the best results, both with $R^2 \geqslant 0.93$.
3. Regression using Frank's cupola reproduces the trend of the fitted laws by including important degrees of uncertainty about the mean, thereby capturing one dimension of the variability in the underlying data. Both fitted laws lie within the range between the first and third quartiles.

In the light of these results, we hope that the statistical characterization of sedimentation velocity will contribute to new modelling perspectives bymoving from deterministic to probabilistic models of saltation and suspension. A number of real world applications related to windblown sand and dust hazards and related risk assessment could benefit from such models. For example, it could be worth assessing the joint uncertainty propagation from sedimentation velocity and friction velocity to transport rate, distribution of particles above a surface, transition thresholds from one mode of transport to another. Finally, for applications where risk assessment is desirable, the ability to attribute likelihood conditions to such predictions will be of critical importance.

Acknowledgments

The study has been partially funded by the European Union within the MSCA-ITN-2016-EID research project Sand Mitigation around Railway Tracks (SMaRT, www.smart-eid.eu). The SMaRT project has received funding from the European Union Horizon 2020 research and innovation program under grant agreement No 721798. In particular, we acknowledge M. Horvat, R. Nuca and L. Preziosi, members of the SMaRT team, for the early discussions about the topic of the study within the SMaRT innovative training programme. The study has been developed in the framework of the Windblown Sand Modelling and Mitigation (WSMM) joint research, development and consulting group established between Politecnico di Torino and Optiflow Company. The present study benefits from a long-term effort made by several authors to measure particle sedimentation velocities: we are grateful to all of them. In particular, we wish to thank Yin Wang and co-workers at Dalian University of Technology, for their generosity in providing experimental data.

References

Achenbach, E., 1974. Vortex shedding from spheres. J. Fluid Mech. 62, 209–221. https://doi.org/10.1017/S0022112074000644.
Alger, G.R., 1964. Terminal fall velocity of particles of irregular shapes as affected by surface area. Ph.D. thesis.
Anderson, R.L., Hallet, B., 1986. Sediment transport by wind: Toward a general model. Geol. Soc. Am. Bull. 97, 523–535. https://doi.org/10.1130/0016-7606(1986)97<523:STBWTA>2.0.CO;2.
Baas, A.C., 2019. Grains in Motion. John Wiley and Son. pp. 27–60.
Baddock, M., Strong, C., Murray, P., McTainsh, G., 2013. Aeolian dust as a transport hazard. Atmos. Environ. 71, 7–14. https://doi.org/10.1016/j.atmosenv.2013.01.042.
Bagheri, G., Bonadonna, C., 2016. On the drag of freely falling non-spherical particles. Powder Technol. 301, 526–544. https://doi.org/10.1016/j.powtec.2016.06.015.
Bagnold, R.A., 1935. The movement of desert sand. Geogr. J. 85, 342–365.
Briggs, L.I., McCulloch, D.S., Moser, F., 1962. The hydraulic shape of sand particles. J. Sediment. Res. 32, 645–656. https://doi.org/10.1306/74D70D44-2B21-11D7-8648000102C1865D.
Brown, P.P., Lawler, D.F., 2003. Sphere drag and settling velocity revisited. J. Environ. Eng. 129, 222–231. https://doi.org/10.1061/(ASCE)0733-9372(2003)129:3(222).
Bruno, L., Horvat, M., Raffaele, L., 2018. Windblown sand along railway infrastructures: a review of challenges and mitigation measures. J. Wind Eng. Ind. Aerodyn. 177, 340–365. https://doi.org/10.1016/j.jweia.2018.04.021.
Chen, W., Fryrear, D.W., 2001. Aerodynamic and geometric diameter of airborne particles. J. Sediment. Res. 71, 365–371. https://doi.org/10.1306/2DC4094A-0E47-11D7-8643000102C1865.
Chen, W., Fryrear, D.W., 2002. Aerodynamic and geometric diameter of airborne particles: Reply. J. Sediment. Res. 72, 442–443. https://doi.org/10.1306/102201720442.
Clift, R., Gauvin, W.H., 1971. Motion of entrained particles in gas streams. Can. J. Chem. Eng. 49, 439–448. https://doi.org/10.1002/cjce.5450490403.
Clift, R., Grace, J.R., Weber, M.E., 2005. Bubbles, Drops, and Particles. Courier corporation ed.
Corey, A.T., 1949. Influence of shape on the fall velocity of sand grains. Msc thesis.
Cox, R.G., 1965. The steady motion of a particle of arbitrary shape at small reynolds numbers. J. Fluid Mech. 23, 625–643. https://doi.org/10.1017/S0022112065001593.
Cui, B., Komar, P.D., Baba, J., 1983. Settling velocities of natural sand grains in air. J. Sediment. Petrol. https://doi.org/10.1306/212F8346-2B24-11D7-8648000102C1865D.
Dietrich, W.E., 1982. Settling velocity of natural particles. Water Resour. Res. 18, 1615–1626. https://doi.org/10.1029/WR018i006p01615.
Dioguardi, F., Mele, D., Dellino, P., 2017. A new one-equation model of fluid drag for irregularly shaped particles valid over a wide range of reynolds number. J. Geophys. Res.: Solid Earth 123, 144–156. https://doi.org/10.1002/2017JB014926.
Ellis, J.T., Sherman, D.J., 2013. Fundamentals of Aeolian Sediment Transport: Windblown Sand, vol. 11 Academic Presshttps://doi.org/10.1016/B978-0-12-374739-6.00299-2. pp. 85–108.
Farrell, E.J., Sherman, D.J., 2013. Estimates of the Schmidt Number for vertical flux distributions of wind-blown sand. J. Coastal Res. 165, 1289–1295. https://doi.org/10.2112/SI65-218.1.
Farrell, E.J., Sherman, D.J., 2015. A new relationship between grain size and fall (settling) velocity in air. Prog. Phys. Geogr. 39, 361–387. https://doi.org/10.1177/0309133314562442.
Ferguson, R.I., Church, M., 2004. A simple universal equation for grain settling velocity. J. Sediment. Res. 74, 933–937. https://doi.org/10.1306/051204740933.
Fernandes, R., Dupont, S., Lamaud, E., 2019. Investigating the role of deposition on the size distribution of near-surface dust flux during erosion events. Aeolian Res. 37, 46–63. https://doi.org/10.1016/j.aeolia.2019.02.002.
Ganser, G.H., 1993. A rational approach to drag prediction of spherical and nonspherical particles. Powder Technol. 77, 143–152. https://doi.org/10.1016/0032-5910(93)80051-B.
Genest, C., Favre, A.C., 2007. Everything you always wanted to know about copula modeling but were afraid to ask. J. Hydrol. Eng. (ASCE) 12, 347–368. https://doi.org/10.1061/(ASCE)1084-0699(2007)12: 4(347).
Genest, C., Nešlehová, J., 2014. Copulas and copula models. In: Wiley StatsRef: Statistics Reference Online. John Wiley & Sons, Ltd. https://doi.org/10.1002/9781118445112.stat07523.
Gillies, J.A., 2013. Fundamentals of Aeolian Sediment Transport: Dust Emissions and Transport – Near Surface, vol. 11 Academic Presshttps://doi.org/10.1016/B978-0-12-374739-6.00297-9. pp. 43–63.
Griffin, D.W., 2007. Atmospheric movement of microorganisms in clouds of desert dust and implications for human health. Clin. Microbiol. Rev. 3, 459–477. https://doi.org/10.1128/CMR.00039-06.

Haider, A., Levenspiel, O., 1989. Drag coefficient and terminal velocity of spherical and nonspherical particles. Powder Technol. 58, 63–70. https://doi.org/10.1016/0032-5910(89)80008-7.
Holze, C., Brucks, A., 2014. Accelerated lifetime modeling on the basis of wind tunnel analysis and sand storm aging. Energy Procedia 49, 1692–1699. https://doi.org/10.1016/j.egypro.2014.03.178.
Ishihara, T., Iwagaki, Y., 1952. On the effect of sand storm in controlling the mouth of the kiku river. Bulletins - Disaster Prevention Research Institute, Kyoto University 2, 1–32.
ISO14688-1:2017, 2017. Geotechnical investigation and testing – identification and classification of soil – part 1: Identification and description.
Jerolmack, D.J., Mohrig, D., Grotzinger, J.P., Fike, D.A., Watters, W.A., 2006. Spatial grain size sorting in eolian ripples and estimation of wind conditions on planetary surfaces: application to meridiani planum, mars. J. Geophys. Res.: Planets 111. https://doi.org/10.1029/2005JE002544.
Ji, S.B., Gerber, A.G., Sousa, A.C.M., 2004. A convection-diffusion CFD model for aeolian particle transport. Int. J. Numer. Meth. Fluids 45, 797–817. https://doi.org/10.1002/fld.724.
Johnson, T.A., Patel, V.C., 1999. Flow past a sphere up to a reynolds number of 300. J. Fluid Mech. 378, 19–70. https://doi.org/10.1017/S0022112098003206.
Kok, J.F., Renno, N.O., 2009. A comprehensive numerical model of steady state saltation (comsalt). J. Geophys. Res. 114, D17204. https://doi.org/10.1029/2009JD011702.
Kok, J.F., Parteli, E.J.R., Michaels, T.I., Karam, D.B., 2012. The physics of wind-blown sand and dust. Rep. Prog. Phys. 75, 106901. https://doi.org/10.1088/0034-4885/75/10/106901.
Komar, P.D., Reimers, C.E., 1978. Grain shape effects on settling rates. J. Geol. 86, 193–209.
Le Roux, J.P., 2002. Aerodynamic and geometric diameter of airborne particles: discussion. J. Sediment. Res. 72, 441–448. https://doi.org/10.1306/110801720441.
Le Roux, J.P., 2005. Determination of drag coefficients in measuring particle diameters: discussion. J. Sediment. Res. 75, 520–521. https://doi.org/10.2110/jsr.2005.041.
Le Roux, J.P., 2014. Fall velocity of multi-shaped clasts. J. Volcanol. Geoth. Res. 130–139. https://doi.org/10.1016/j.jvolgeores.2014.11.001.
Li, J., Kandakji, T., Lee, J., Tatarko, J., Blackwell, J., Gill, T., Collins, J., 2018. Blowing dust and highway safety in the southwestern united states: characteristics of dust emission “hotspots” and management implications. Sci. Total Environ. 621, 1023–1032. https://doi.org/10.1016/j.scitotenv.2017.10.124.
Loth, E., 2008. Drag of non-spherical solid particles of regular and irregular shape. Powder Technol. 182, 342–353. https://doi.org/10.1016/j.powtec.2007.06.001.
Malcolm, L., Raupach, M., 1991. Measurements in an air settling tube of the terminal velocity distribution of soil material. J. Geophys. Res. 96, 15275–15286. https://doi.org/10.1029/91JD01198.
Marticorena, B., Formenti, P., 2013. Fundamentals of aeolian sediment transport: long-range transport of dust. vol. 11. pp. 64–84. https://doi.org/10.1016/B978-0-12-374739-6.00298-0.
Mass, C.F., Portman, D.A., 1989. Major volcanic eruptions and climate: a critical evaluation. J. Clim. 2, 566–593. https://doi.org/10.1175/1520-0442(1989)002<0566:MVEACA>2.0.CO;2.
McCormick, M.P., Thomason, L.W., Trepte, C.R., 1995. Atmospheric effects of the Mt Pinatubo eruption. Nature 373, 399–404. https://doi.org/10.1038/373399a0.
McTainsh, G., Livingstone, I., Strong, C., 2013. Fundamentals of aeolian sediment transport: aeolian sediments. Fundamentals of Aeolian Sediment Transport: Aeolian Sediments, vol. 11 Academic Presshttps://doi.org/10.1016/B978-0-12-374739-6.00296-7. pp. 23–42.
Middleton, N., 2017. Desert dust hazards: a global review. Aeolian Res. 24, 53–63. https://doi.org/10.1016/j.aeolia.2016.12.001.
Nelsen, R.B., 2007. An Introduction to Copulas. Springer Series in Statistics. Springer-Verlaghttps://doi.org/10.1007/0-387-28678-0.
Newton, I., 1687. Philosophiae naturalis principia mathematica.
Nickling, W.G., McKenna Neuman, C., 2009. Geomorphology of Desert Environments. Springer: Netherlands. chapter Aeolian sediment transport. pp. 517–555. https://doi.org/10.1007/978-1-4020-5719-9.
Owen, P.R., 1964. Saltation of uniform grains in air. J. Fluid Mech. 20, 225–242. https://doi.org/10.1017/S0022112064001173.
Paz, C., Suárez, E., Gil, C., Concheiro, M., 2015. Numerical study of the impact of windblown sand particles on a high-speed train. J. Wind Eng. Ind. Aerodyn. 145, 87–93. https://doi.org/10.1016/j.jweia.2015.06.008.
Pischiutta, M., 2012. Mathematical and numerical modelling of the evolution of mixtures of sand in aeolian dunes. Ph.D. thesis.
Preziosi, L., Fransos, D., Bruno, L., 2015. A multiphase first order model for non-equilibrium sand erosion, transport and sedimentation. Appl. Math. Lett. 45, 69–75. https://doi.org/10.1016/j.aml.2015.01.011.
Pye, K., Tsoar, H., 2009. Aeolian Sand and Sand Dunes. Springerhttps://doi.org/10.1007/978-3-540-85910-9.
Raffaele, L., Bruno, L., Pellerey, F., Preziosi, L., 2016. Windblown sand saltation: a statistical approach to fluid threshold shear velocity. Aeolian Res. 23, 79–91. https://doi.org/10.1016/j.aeolia.2016.10.002.
Rivas Jr, J.A., Mohl, J.E., Van Pelt, R.S., Leung, M.Y., Wallace, R.L., Gill, T.E., Walsh, E.J., 2018. Evidence for regional aeolian transport of freshwater micrometazoans in arid regions. Limnol. Oceanogr. Lett. 3, 320–330. https://doi.org/10.1002/lol2.10072.
Romanovskiy, V.V., 1966. A study of the fall velocity of coarse sediment. Soviet Hydrol.: Selected Papers 47–62.
Rouse, H., 1938. Fluid Mechanics for Hydraulic Engineers.
Rouse, H., 1938b. Nomogram for the settling velocity of spheres (Technical Report). National Research Council.
Sadegh, M., Ragno, E., AghaKouchak, A., 2017. Multivariate copula analysis toolbox (mvcat): describing dependence and underlying uncertainty using a bayesian framework. Water Resour. Res. 53. https://doi.org/10.1002/2016WR020242.
Schulz, E.F., Wilde, R.H., Albertson, M.L., 1954. Influence of shape on the fall velocity of sedimentary particles. MRD Sediment Series.
Shao, Y., 2008. Physics and Modelling of Wind Erosion. Springerhttps://doi.org/10.1007/978-1-4020-8895-7.
Stokes, G.G., 1851. On the Effect of the Internal Friction of Fluids on the Motion of Pendulums, vol. 9 Pitt Press, Cambridge.
Stringham, G.E., Simons, D.B., Guy, H.P., 1969. The behavior of large particles falling in quiescent liquids. https://doi.org/10.3133/pp562C.
Sundborg, A., 1955. Meteorological and climatological conditions for the genesis of aeolian sediments. Geogr. Ann. 37, 94–111.
Tomboulides, A.G., Orszag, S.A., 2000. Numerical investigation of transitional and weak turbulent flow past a sphere. J. Fluid Mech. 416, 45–73. https://doi.org/10.1017/S0022112000008880.
Tran-Cong, S., Gay, M., Michaelides, E.E., 2004. Drag coefficients of irregularly shaped particles. Powder Technol. 139, 21–32. https://doi.org/10.1016/j.powtec.2003.10.002.
Udo, K., Mano, A., 2011. Application of rouse’s sediment concentration profile to aeolian transport: is the suspension system for sand transport in air the same as that in water? J. Coastal Res. 2079–2083.
Valence, A., Rasmussen, K.R., El Moctar, A.O., Dupont, P., 2015. The physics of Aeolian sand transport. C.R. Phys. 16, 105–117. https://doi.org/10.1016/j.crhy.2015.01.006.
Wang, Z., Ren, S., Huang, N., 2014. Saltation of non-spherical sand particles. PLoS ONE 9, e105208. https://doi.org/10.1371/journal.pone.0105208.
Wang, Y., Zhou, L., Wu, Y., Yang, Q., 2018. New simple correlation formula for the drag coefficient of calcareous sand particles of highly irregular shape. Powder Technol. 326, 379–398. https://doi.org/10.1016/j.powtec.2017.12.004.
White, B.R., Lacchia, B.M., Greeley, R., Leach, R.N., 1997. Aeolian behavior of dust in a simulated martian environment. J. Geophys. Res.: Planets 102, 25629–25640. https://doi.org/10.1029/97JE01753.
Wilde, R.H., 1952. Effect of shape on the fall-velocity of grand-sized particles.
Wilson, L., Huang, T., 1979. The influence of shape on the atmospheric settling velocity of volcanic ash particles. Earth Planet. Sci. Lett. 44, 311–324. https://doi.org/10.1016/0012-821X(79)90179-1.
Yizhaq, H., Katra, I., 2015. Longevity of aeolian megaripples. Earth Planet. Sci. Lett. 422, 28–32. https://doi.org/10.1016/j.epsl.2015.04.004.
Zio, E., Pedroni, N., 2013. Literature Review of Methods for Representing Uncertainty. Foundation for an Industrial Safety Culture.